Microbiology (2005), **151**, 693–706 DOI 10.1099/mic.0.27481-0

Metabolic flux analysis of *Escherichia coli* in glucose-limited continuous culture. I. Growth-rate-dependent metabolic efficiency at steady state

Anke Kayser,† Jan Weber,‡ Volker Hecht and Ursula Rinas

Biochemical Engineering Division, GBF – National Research Centre for Biotechnology, Mascheroder Weg 1, 38124 Braunschweig, Germany

Correspondence
Ursula Rinas
URI@gbf.de

Received 12 July 2004
Revised 3 December 2004
Accepted 6 December 2004

The *Escherichia coli* K-12 strain TG1 was grown at 28 °C in aerobic glucose-limited continuous cultures at dilution rates ranging from 0·044 to 0·415 h^{-1}. The rates of biomass formation, the specific rates of glucose, ammonium and oxygen uptake and the specific carbon dioxide evolution rate increased linearly with the dilution rate up to 0·3 h^{-1}. At dilution rates between 0·3 h^{-1} and 0·4 h^{-1}, a strong deviation from the linear increase to lower specific oxygen uptake and carbon dioxide evolution rates occurred. The biomass formation rate and the specific glucose and ammonium uptake rates did not deviate that strongly from the linear increase up to dilution rates of 0·4 h^{-1}. An increasing percentage of glucose carbon flow towards biomass determined by a reactor mass balance and a decreasing specific ATP production rate concomitant with a decreasing adenylate energy charge indicated higher energetic efficiency of carbon substrate utilization at higher dilution rates. Estimation of metabolic fluxes by a stoichiometric model revealed an increasing activity of the pentose phosphate pathway and a decreasing tricarboxylic acid cycle activity with increasing dilution rates, indicative of the increased NADPH and precursor demand for anabolic purposes at the expense of ATP formation through catabolic activities. Thus, increasing growth rates first result in a more energy-efficient use of the carbon substrate for biomass production, i.e. a lower portion of the carbon substrate is channelled into the respiratory, energy-generating pathway. At dilution rates above 0·4 h^{-1}, close to the wash-out point, respiration rates dropped sharply and accumulation of glucose and acetic acid was observed. Energy generation through acetate formation yields less ATP compared with complete oxidation of the sugar carbon substrate, but is the result of maximized energy generation under conditions of restrictions in the tricarboxylic acid cycle or in respiratory NADH turnover. Thus, the data strongly support the conclusion that, in aerobic glucose-limited continuous cultures of *E. coli* TG1, two different carbon limitations occur: at low dilution rates, cell growth is limited by cell-carbon supply and, at high dilution rates, by energy-carbon supply.

INTRODUCTION

Escherichia coli is the most common micro-organism used for the production of various recombinant compounds such as heterologous proteins. It offers the advantage of growing at predetermined growth rates to high cell densities by simple fed-batch techniques using defined media with inexpensive carbon sources such as glucose or glycerol (Riesenberg *et al.*, 1991; Korz *et al.*, 1995). Depending on culture conditions, growth yields on these carbon substrates can differ considerably, reflecting the variable efficiency with which aerobic-growing *E. coli* generates energy via substrate-level and oxidative phosphorylation and subsequently utilizes this energy for biosynthetic purposes. Experimentally determined values of the ATP requirements for biosynthesis of cell material are in general much higher than values determined by theoretical studies (e.g. Farmer & Jones, 1976), indicating a partial uncoupling of energy-conserving and energy-utilizing cellular reactions.

As protein synthesis, or more specifically the polymerization of amino acids, is the biggest energy-consuming process in the cell, with more than 50 % of the ATP consumption for biosynthetic purposes (Stouthamer, 1973), energy generation may become critical in recombinant-protein-overproducing cells. For example, the metabolic burden of

†Present address: DSM Biologics, 6000 av. Royalmount, Montréal, Quebec, Canada H4P 2T1.

‡Present address: Aventis Pharma Deutschland GmbH (ein Unternehmen der sanofi-aventis Gruppe), 65926 Frankfurt, Germany.

Abbreviations: AEC, adenylate energy charge; CTR, carbon dioxide transfer rate; EMP, Embden–Meyerhof–Parnas; MG, methylglyoxal; OTR, oxygen transfer rate; PP, pentose phosphate.

recombinant protein production is manifested in an increased respiratory activity, i.e. in an increased activity of the energy-generating pathway (e.g. Hoffmann & Rinas, 2001; Weber *et al.*, 2002). To understand and control the producing cell better, it is important to have a more profound knowledge of how the cell couples energy generation and carbon supply in the catabolic pathways with the anabolic requirements at different growth rates under non-producing conditions.

It appears reasonable to assume that, in a balanced growing cell, fuelling and biosynthetic reactions are fine-tuned in such a way that cells grow at the highest possible rate under given conditions. This assumption is supported by the good agreement of calculated flux distributions with experimental data using 'maximize growth' as an objective function in a linear programming environment (e.g. Varma & Palsson, 1993). 'Maximize growth' implies optimum energy generation in catabolic reaction sequences and an optimum drain of biosynthetic precursors for anabolic demands.

Information on metabolic fluxes can be obtained from a metabolic model and a set of measured fluxes, typically the uptake rates of substrates and secretion rates of metabolites (Vallino & Stephanopoulos, 1990). The analysis relies on the stoichiometry of cellular pathways, the metabolic demand for growth and optimization principles to estimate the intracellular carbon flux within the defined network. These stoichiometry-based metabolic models have been applied to a variety of organisms, including *E. coli* (Varma & Palsson, 1993; Pramanik & Keasling, 1997). The calculated flux distributions are based on a pseudo-steady state assumption for intracellular metabolites, which is best verified at steady state in continuous culture.

In this study, the effect of growth rate on catabolic and anabolic fluxes and energetic efficiency of the *E. coli* K-12 strain TG1 growing in aerobic glucose-limited continuous culture was examined. Moreover, the energetic state of the cells was analysed by measurement of the intracellular adenosine nucleotide pool.

METHODS

Micro-organism and medium. The *E. coli* K-12 strain TG1 (=DSM 6056) was grown on a defined medium with (per litre) 11 g glucose monohydrate (corresponding to 10 g glucose), 8 g $(NH_4)_2SO_4$, 0·8 g $(NH_4)_2HPO_4$, 2·7 g KH_2PO_4, 0·35 g citric acid monohydrate, 1 g $MgSO_4.7H_2O$, 12 mg ferric citrate, 0·5 mg $CoCl_2.6H_2O$, 3 mg $MnCl_2.4H_2O$, 0·3 mg $CuCl_2.2H_2O$, 0·6 mg H_3BO_3, 0·5 mg $Na_2MoO_4.2H_2O$, 1·6 mg $Zn(CH_3COO)_2.2H_2O$, 1·7 mg EDTA and 4 mg thiamine. Glucose and magnesium sulfate were autoclaved separately. Thiamine was added by sterile filtration.

Cultivation conditions. Continuous cultivations were performed at 28 °C, at a stirring speed of 800 r.p.m., and the pH was controlled at pH 6·6 with 2·5 mol NaOH l^{-1}. The 2-l bioreactor (model SGI 7F-Set2; Setric) was equipped with standard measuring and control units (temperature, pH, dissolved oxygen, stirrer speed). A constant aeration rate of 1·33 v.v.m. was achieved by a mass flow controller (Brooks). Continuous cultivation was performed for at least eight residence times at a given dilution rate; steady-state conditions were verified by constant optical density and oxygen and carbon dioxide transfer rates. Except for glucose, all other substrates were in excess. The concentration of dissolved oxygen was always maintained above 20 % of air saturation.

Analytical techniques. Culture liquid was withdrawn from the bioreactor into an ice-cooled beaker. Cell dry mass was determined gravimetrically after centrifugation of a known sample volume. The pellet was washed twice with 0·9 % w/v NaCl and dried at 40 °C under vacuum for 48 h. Elemental biomass composition was analysed with a PE 2400 II elemental analyser (Perkin Elmer). Glucose was measured enzymically by a YSI glucose analyser (model 2700; Yellow Springs Instrument Co.). Organic acids, i.e. acetic acid, formic acid, lactic acid and pyruvic acid, were analysed by HPLC using an HPX-87H Aminex ion-exclusion column (Bio-Rad). The column, connected to a UV detector ($\lambda = 210$ nm) and RI detector, was eluted at 50 °C with 5 mmol H_2SO_4 l^{-1} at a flow rate of 0·5 ml min^{-1}.

Ammonium concentrations were analysed by an ammonium electrode (model Orion 95-12; Colora).

The concentrations of oxygen and carbon dioxide in the off-gas were measured by paramagnetic and infrared gas analysis systems, respectively (Maihak).

For determination of the adenosine nucleotides AMP, ADP and ATP, 3–5 ml cell suspension was taken from the bioreactor using a rapid sampling device (described in Theobald *et al.*, 1997). Since turnover of the adenosine nucleotide pool occurs in a few seconds (Nielsen & Villadsen, 1994; p. 55ff.), a fast sampling technique was necessary to inactivate metabolic activities immediately. Briefly, samples were removed from the bioreactor through a capillary needle into evacuated sample tubes containing precooled glass beads in 5 mol perchloric acid l^{-1} (−25 °C) for immediate inactivation of cell metabolism. One freeze–thaw cycle between 0 °C and −25 °C was performed. The extract was neutralized on ice by careful addition of 2 mol KOH l^{-1} and insoluble cell debris was removed by centrifugation (14 000 r.p.m., 15 s; Eppendorf model 5417) and subsequent membrane filtration (pore size 0·45 μm). Neutralized samples were analysed by ion-pair HPLC, using a reversed-phase column (Supelcosil LC-18T; Supelco) with tetrabutylammonium hydrogensulfate as pairing agent and methanol pH-gradient elution (Ryll & Wagner, 1991).

Mass balances, calculations and flux analysis. Volumetric oxygen and carbon dioxide transfer rates (OTR and CTR, respectively) were calculated from the mass balance of the gas phase as follows:

$$\mathrm{OTR} = \frac{M_{O_2} \cdot F_G^{in}}{V(t) \cdot V_M} \left(x_{O_2}^{in}(t) - x_{O_2}^{out}(t) \cdot \frac{1 - x_{O_2}^{in}(t) - x_{CO_2}^{in}(t)}{1 - x_{O_2}^{out}(t) - x_{CO_2}^{out}(t)} \right) \quad (1)$$

and

$$\mathrm{CTR} = \frac{M_{CO_2} \cdot F_G^{in}}{V(t) \cdot V_M} \left(x_{CO_2}^{out}(t) \cdot \frac{1 - x_{O_2}^{in}(t) - x_{CO_2}^{in}(t)}{1 - x_{O_2}^{out}(t) - x_{CO_2}^{out}(t)} - x_{CO_2}^{in}(t) \right) \quad (2)$$

where M_{O_2} and M_{CO_2} are the molecular mass of oxygen and carbon dioxide (g mol^{-1}), respectively, F_G^{in} the volumetric inlet air flow (l h^{-1}) at standard conditions, V(t) the working volume of the bioreactor (l), V_M the mol volume of the ideal gas (l mol^{-1}) at standard conditions, $x_{O_2}^{in}$ (t) and $x_{CO_2}^{in}$ (t) the molar fractions of oxygen and carbon dioxide (mol mol^{-1}), respectively, in the inlet air, and $x_{O_2}^{out}$ (t) and $x_{CO_2}^{out}$ (t) the molar fractions of oxygen and carbon dioxide (mol mol^{-1}), respectively, in the outlet air of the bioreactor. For calculation of specific rates, the convective

flow of oxygen and carbon dioxide was neglected and the volumetric transfer rates OTR and CTR were considered to be identical to the volumetric oxygen uptake and carbon dioxide evolution rates, respectively. Specific rates were calculated by dividing volumetric rates by cell concentration.

Carbon (C_{rec}) and nitrogen (N_{rec}) recoveries at steady-state conditions were determined from reactor mass balances according to the following equations:

$$C_{rec} = \frac{\alpha_{CBiomass} \cdot D \cdot C_{Biomass} + \alpha_{CGlucose} \cdot D \cdot C_{Glucose} + \alpha_{CAcetate} \cdot D \cdot C_{Acetate} + \alpha_{CO_2} \cdot CTR}{\alpha_{CGlucose} \cdot D \cdot C^0_{Glucose}} \quad (3)$$

and

$$N_{rec} = \frac{\alpha_{NBiomass} \cdot C_{Biomass} + \alpha_{NNH_4} \cdot C_{NH_4}}{\alpha_{NNH_4} \cdot C^0_{NH_4}} \quad (4)$$

where α_{ij} is the mass fraction of element i in compound j (g g^{-1}), D the dilution rate (h^{-1}), C_j the concentration of compound j in the bioreactor and C^0_j the concentration of compound j in the feeding solution. For the calculation of $\alpha_{CBiomass}$ and $\alpha_{NBiomass}$, the elemental biomass composition was determined as $CH_{1{\cdot}85}O_{0{\cdot}574}N_{0{\cdot}22}$ plus 12 % ash. The elemental biomass composition did not change with the dilution rate (data not shown).

The adenylate energy charge (AEC) was calculated from the adenosine nucleotide pool measurement according to the definition given by Atkinson (1968):

$$AEC = \frac{C_{ATP} + 0{\cdot}5 \cdot C_{ADP}}{C_{ATP} + C_{ADP} + C_{AMP}} \quad (5)$$

where C_{ATP}, C_{ADP} and C_{AMP} respectively represent the intracellular concentrations of the adenosine nucleotides ATP, ADP and AMP.

Stoichiometrically derived mass balances were used to estimate the carbon flux through the central metabolic pathways (Vallino & Stephanopoulos, 1990; van Gulik & Heijnen, 1995). The biochemical reactions and considered metabolites form a set of linear equations which can be expressed in matrix notation as:

$$A.x = r \quad (6)$$

with the stoichiometric matrix A, the vector of unknown fluxes x and the vector r of the accumulation rates. Assuming pseudo-steady state for intracellular metabolites, the respective accumulation rates can be set to zero. The generated bioreaction network was underdetermined (number of reactions greater than the number of metabolites). Because multiple solutions exist for underdetermined networks, linear programming (optimization) was used to determine the flux distribution (for details of the method see Varma & Palsson, 1994; van Gulik & Heijnen, 1995; Pramanik & Keasling, 1997). Numerical values for the unknown fluxes were obtained with the following constraints; (i) fixing the specific glucose uptake rate, (ii) specifying the direction of the reaction according to its thermodynamic property, specifying the energetic parameters P/O ratio, $Y_{X/ATP}$ and m_{ATP} as described in the Results and Discussion section and by defining an objective function. The objective function was defined as 'maximize growth':

$$Z = -r_{biomass} \rightarrow \text{minimize} \quad (7)$$

Linear programming was carried out using a two-phase simplex algorithm (MATLAB, version 4.2c.1; The MathWorks). The metabolic network was constructed on basis of the *E. coli* database EcoCyc (Karp *et al.*, 1999; http://BioCyc.org/ecocyc/); anabolic reactions for biomass synthesis including polymerization, biosynthesis, fuelling reactions and transport are based on data given by Ingraham *et al.* (1983). The network contains 102 reactions and 90 metabolites and is listed in the Appendix. It includes reactions of the central metabolic pathways, i.e. the Embden–Meyerhof–Parnas (EMP) pathway, the tricarboxylic acid (TCA) cycle, the pentose phosphate (PP) pathway, the methylglyoxal (MG) pathway and gluconeogenesis. Anaplerotic pathways detected in *E. coli* include reactions catalysed by phosphoenolpyruvate (PEP) carboxylase, PEP carboxykinase, an NAD- and NADP-specific malate enzyme and isocitrate lyase and malate synthase of the glyoxylate shunt. In *E. coli*, two different types of pyridine dinucleotide transhydrogenase exist for the interconversion of NADPH and NADH: a membrane-bound energy-dependent transhydrogenase (Bragg *et al.*, 1972; Rydström, 1977) and a soluble cytoplasmic transhydrogenase involved in the energy-independent transfer of hydride from NADPH to NAD^+ (Boonstra *et al.*, 1999). Oxidative phosphorylation was accounted for by an energy- and non-energy-linked NADH dehydrogenase, an FADH reductase and a formate dehydrogenase reaction. Some reactions in linear metabolic routes were lumped together, i.e. anabolic reactions concerning nucleotide and lipid metabolism and the synthesis of several amino acids. The biomass equation was adapted to the macromolecular composition of *E. coli*. The values 3·1 % DNA, 9·1 % lipids, 3·4 % lipopolysaccharide, 2·5 % peptidoglycan and 2·5 % glycogen (% w/w) were taken from Ingraham *et al.* (1983). Values for protein, 62 %, and RNA, 11·5 %, were obtained from our own measurements according to the methods described by Herbert *et al.* (1971) and Benthin *et al.* (1991), respectively. Metabolic fluxes were calculated on a molar basis and for biomass we have considered the amounts required for the formation of 100 g biomass. The stoichiometries used in the lumped biomass equation (r93; see Appendix, detailed stoichiometric model) were adjusted accordingly. This way, for the convenience of modelling, we virtually consider a 'molecular mass of the biomass' corresponding to 100 g mol^{-1}.

Although the macromolecular biomass composition changes with the growth rate (Shahab *et al.*, 1996), it was considered constant as the impact of these changes on the intracellular flux distributions is negligible, as has been shown by a sensitivity analysis (data not shown; Daae & Ison, 1999).

RESULTS AND DISCUSSION

Growth yields and energetics: the classical approach using a simple stoichiometric model

Aerobic glucose-limited continuous steady-state cultures with dilution rates ranging from D = 0·044 to 0·415 h^{-1} were used to determine the growth parameters of *E. coli* TG1. The concentrations of biomass, glucose and acetate and the volumetric CTR as a function of the dilution rate are shown in Fig. 1 (also summarized in Table 1). At dilution rates above 0·4 h^{-1}, the concentrations of glucose and acetate increased considerably concomitant with a strong decrease in the biomass concentration and the volumetric CTR, clearly showing that growth at these dilution rates was close to the wash-out point. All data obtained from steady-state cultures were tested for consistency by applying a reactor mass balance for the elements carbon and nitrogen (Table 1). The nitrogen recovery was always above 97 %; a satisfactory carbon recovery, however, was only obtained for dilution rates up to 0·4 h^{-1}, which prompted us to omit the data of the two steady states at dilution rates above 0·4 h^{-1} (shaded area in Fig. 1) from further calculations.

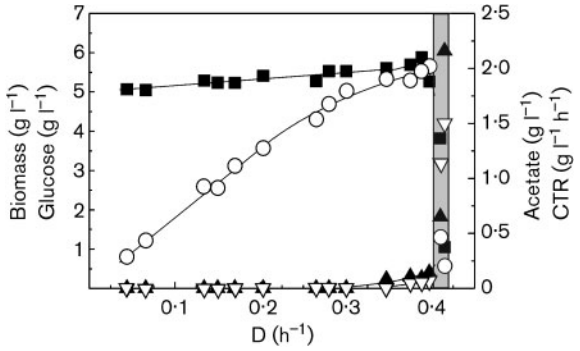

Fig. 1. Glucose-limited continuous culture of *E. coli* TG1. The concentrations of biomass (■), glucose (▲) and acetate (▽) and the volumetric CTR (○) are shown as functions of the dilution rate D. The shaded area corresponds to dilution rates above 0·4 h^{-1} close to the wash-out point, with a decreasing biomass concentration and CTR concomitant with the accumulation of glucose and acetate.

According to the maintenance model of Pirt (1965), the specific rates r_j of substrate uptake and product formation can be expressed as linear functions of the dilution rate (which equals the specific growth rate μ at steady state) by ascribing the consumption of a given substrate (or the formation of a product) to a growth-associated and a non-growth-associated process:

$$r_j = \frac{\mu}{Y_j^{\text{true}}} + m_j \qquad (8)$$

where Y_j^{true} is the true yield coefficient (g g^{-1}) not considering any maintenance-associated processes and m_j the maintenance term (g g^{-1} h^{-1}).

At dilution rates below 0·3 h^{-1}, the specific uptake rates for glucose, ammonium and oxygen and the specific carbon dioxide evolution rate increased linearly with the dilution rate while acetate formation was not observed (Fig. 2; see also data in Table 2). At dilution rates between 0·3 h^{-1} and 0·4 h^{-1}, a strong deviation from the linear increase to lower specific oxygen uptake and carbon dioxide evolution rates occurred (Fig. 2a). This strong deviation from the linear increase to lower rates was not observed for the biomass formation rate and the specific uptake rates of glucose and ammonium (Fig. 2a and b, respectively). In contrast, the biomass formation (Fig. 2a) and the specific ammonium uptake (Fig. 2b) rates even revealed a small deviation from the linear increase towards higher rates, while the specific glucose uptake rate (Fig. 2b) revealed a slightly decreasing deviation from the linear increase with increasing dilution rates. In summary, these results point to a higher efficiency of nitrogen and carbon incorporation into biomass, i.e. more efficient substrate utilization for growth, at dilution rates between 0·3 h^{-1} and 0·4 h^{-1}. From the linear range of the specific glucose uptake rate as a function of the dilution rate (r_{Glucose}, D = 0→0·347 h^{-1}), the growth-associated stoichiometric true yield coefficient $Y_{\text{Glucose}}^{\text{true}}$ and the non-growth-associated maintenance coefficient m_{Glucose} were determined according to equation 8 as 0·57 g g^{-1} and 0·02 g g^{-1} h^{-1}, respectively.

Detectable levels of acetate were first observed at a growth rate of 0·375 h^{-1} (50 mg l^{-1}, Fig. 1) and between D = 0·375 h^{-1} and 0·4 h^{-1} acetate formation rates increased

Table 1. Concentrations of biomass, glucose, acetate and ammonium and volumetric CTR and OTR during steady-state growth of *E. coli* TG1 at various dilution rates in glucose-limited continuous cultures

Data consistency was analysed by determination of the carbon and nitrogen recoveries by applying reactor mass balances.

D (h^{-1})	Concentrations (g l^{-1})				CTR (g l^{-1} h^{-1})	OTR (g l^{-1} h^{-1})	Recovery (%)	
	Biomass	Glucose	Acetate	Ammonium			Carbon	Nitrogen
0·044	5·07	0·000	0·000	1·709	0·286	0·222	96	99
0·066	5·05	0·000	0·000	1·688	0·440	0·288	97	98
0·134	5·29	0·000	0·000	1·652	0·924	0·576	101	98
0·150	5·24	0·000	0·000	1·650	0·915	0·615	95	98
0·170	5·23	0·000	0·000	1·656	1·113	0·896	98	98
0·203	5·41	0·000	0·000	1·629	1·276	0·950	98	98
0·265	5·28	0·000	0·000	1·632	1·536	1·044	93	97
0·280	5·53	0·000	0·000	1·620	1·676	1·226	97	98
0·300	5·53	0·000	0·000	1·612	1·795	1·312	97	98
0·347	5·61	0·229	0·000	1·617	1·905	1·357	96	99
0·375	5·69	0·295	0·048	1·590	1·888	1·373	95	98
0·388	5·88	0·259	0·051	1·556	1·971	1·434	97	98
0·397	5·27	0·398	0·062	1·635	2·015	1·387	93	97
0·410	3·82	1·822	1·140	1·835	0·462	0·330	76	98
0·415	1·05	6·048	1·500	2·245	0·207	0·147	89	99

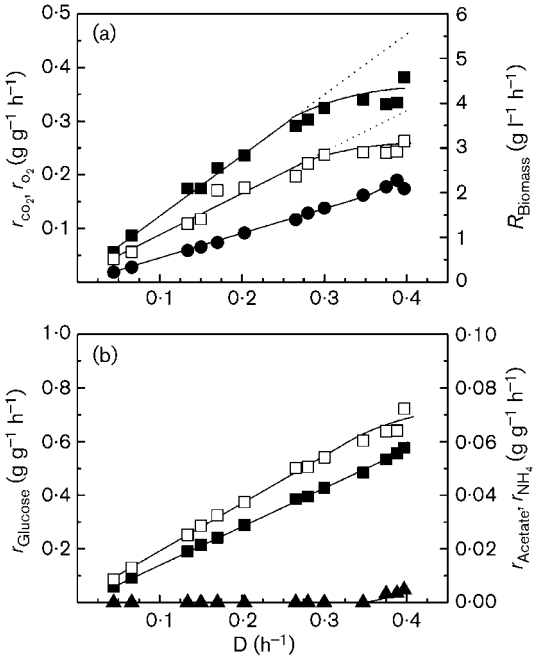

Fig. 2. Substrate uptake and biomass and product formation rates during glucose-limited continuous culture of *E. coli* TG1. (a) The biomass formation rate $R_{Biomass}$ (●) and the specific oxygen uptake r_{O_2} (□) and carbon dioxide evolution rate r_{CO_2} (■) and (b) the specific uptake rate of glucose $r_{Glucose}$ (□) and ammonium r_{NH_4} (■) and the specific formation rate of acetate $r_{Acetate}$ (▲) were calculated as functions of the dilution rate D. Data from dilution rates above 0·4 h^{-1} were omitted from these calculations.

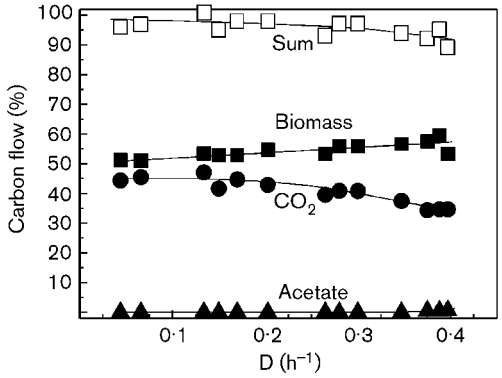

Fig. 3. Carbon mass balance during glucose-limited continuous culture of *E. coli* TG1. The percentage of glucose carbon flow towards biomass (■), carbon dioxide (●) and acetate (▲) as functions of the dilution rate D. Data from dilution rates above 0·4 h^{-1} were omitted from these calculations.

slightly with the increase in the dilution rate (Fig. 2b). Pronounced accumulation of acetate was observed for dilution rates above 0·4 h^{-1} (Fig. 1).

For calculation of the percentage of glucose carbon flow towards biomass, carbon dioxide and acetate, the data from the reactor mass balance (Table 1) were expressed on a molar basis of carbon atoms, i.e. percentage of carbon atoms from glucose converted to biomass, carbon dioxide and acetate (Fig. 3). This analysis additionally corroborated the decreasing flux of glucose carbon towards carbon dioxide and an increasing flux towards biomass, suggesting a

Table 2. Biomass formation rate and the specific rates of glucose uptake, carbon dioxide evolution, oxygen uptake, acetate formation and ammonium uptake during steady-state growth of *E. coli* TG1 at various dilution rates in glucose-limited continuous cultures

$R_{Biomass}$, Biomass formation rate; $r_{Glucose}$, glucose uptake rate; r_{CO_2}, carbon dioxide evolution rate; r_{O_2}, oxygen uptake rate; $r_{Acetate}$, acetate formation rate; r_{NH_4}, ammonium uptake rate.

D (h^{-1})	$R_{Biomass}$ (g l^{-1} h^{-1})	$r_{Glucose}$ (g g^{-1} h^{-1})	r_{CO_2} (g g^{-1} h^{-1})	r_{O_2} (g g^{-1} h^{-1})	$r_{Acetate}$ (g g^{-1} h^{-1})	r_{NH_4} (g g^{-1} h^{-1})
0·044	0·223	0·087	0·056	0·0437	0·0 000	0·0060
0·066	0·333	0·131	0·087	0·0570	0·0 000	0·0093
0·134	0·709	0·253	0·175	0·1089	0·0 000	0·0190
0·150	0·785	0·287	0·175	0·1175	0·0 000	0·0215
0·170	0·889	0·325	0·213	0·1713	0·0 000	0·0242
0·203	1·098	0·375	0·236	0·1757	0·0 000	0·0289
0·265	1·399	0·502	0·291	0·1978	0·0 000	0·0385
0·280	1·548	0·506	0·303	0·2216	0·0 000	0·0395
0·300	1·659	0·542	0·325	0·2372	0·0 000	0·0427
0·347	1·945	0·605	0·340	0·2421	0·0 000	0·0485
0·375	2·132	0·640	0·332	0·2415	0·0032	0·0534
0·388	2·281	0·643	0·335	0·2438	0·0034	0·0557
0·397	2·092	0·723	0·382	0·2633	0·0047	0·0577

more energy-efficient utilization of the carbon substrate for biomass formation with increasing growth rates. The trend of decreasing carbon recovery with increasing growth rates considering only the formation of biomass, carbon dioxide and acetate might be caused by the formation of an unidentified by-product(s).

In analogy to the maintenance model of Pirt (1965) (equation 8), the growth energetics can be described by balancing the formation and consumption of ATP (Bauchop & Elsden, 1960; Stouthamer & Bettenhaussen, 1973):

$$r_{ATP} = \frac{\mu}{Y_{X/ATP}} + m_{ATP} \quad (9)$$

Again, ATP consumption is ascribed to growth- and non-growth-associated processes, with $Y_{X/ATP}$ as the parameter describing the growth-associated ATP requirements (g mol^{-1}) and m_{ATP} as the maintenance term describing ATP requirement in the absence of growth (mol g^{-1} h^{-1}). A simple stoichiometric model including catabolic and anabolic reactions as listed in the Appendix was used to determine the energetic parameters $Y_{X/ATP}$ (equation 12) and m_{ATP} (equation 13). For the P/O ratio, a value of 1·75 was assumed as determined for enterobacteria (Zeng *et al.*, 1990). Furthermore, the values for the growth-associated stoichiometric true yield coefficient $Y^{true}_{X/Glucose}$ and the non-growth-associated maintenance coefficient $m_{Glucose}$ determined from the linear range of the glucose uptake rate as described above were used as input parameters (see Appendix). Based on this simple stoichiometric model, the ATP consumption for maintenance requirements in the absence of growth m_{ATP} was determined as 2·81 mmol g^{-1} h^{-1} and the growth-associated energy consumption $Y_{X/ATP}$ as 11·6 g mol^{-1}. The above values are in the range of previously reported values determined from aerobic glucose-limited chemostat cultures for growth-associated ATP requirements $Y_{X/ATP}$ (13·9 g mol^{-1} at 30 °C; Farmer & Jones, 1976) and ATP consumption for maintenance m_{ATP} of non-growing cells (2 mmol g^{-1} h^{-1} at 30 °C; Farmer & Jones, 1976).

Growth energetics and metabolic flux distributions: a linear programming approach using a detailed stoichiometric model

The simple stoichiometric model can give a rough estimate of the growth energetics in the linear range of glucose uptake rates, not taking into account any change in the energetic efficiency of growth-rate-dependent variations of energy requirements for biomass formation. Moreover, it should be noted that the P/O ratio, $Y_{X/ATP}$ and m_{ATP} can neither be measured directly nor evaluated independently. A feasible approach to tackle this problem is to set two of these variables as constant and adjust the third to meet experimentally determined data. Thus, the P/O ratio was considered constant as P/O = 1·75 (Zeng *et al.*, 1990) and m_{ATP} was defined as the energy requirement for maintenance in the absence of growth and determined as m_{ATP} = 2·81 mmol g^{-1} h^{-1} (simple stoichiometric model; this study). The values of $Y_{X/ATP}$ were calculated by adjusting their values to reach the experimentally determined biomass yield $Y_{X/Glucose}$ (Table 3) using the detailed stoichiometric model (see Appendix) constructed for estimation of the intracellular carbon flux distribution. Thus, based on the glucose uptake rate, the intracellular fluxes were calculated by linear programming with 'maximize growth' as the objective function, keeping the energetic parameters P/O and m_{ATP} constant and adjusting the third energetic parameter $Y_{X/ATP}$ (present in the biomass formation reaction; r97) to be compatible with the experimentally determined biomass yield $Y_{X/Glucose}$ (Table 3).

Table 3. Growth energetics during glucose-limited continuous cultures

The ATP formation rate r_{ATP} was calculated according to equation 9 by adjustment of the growth-associated ATP consumption $Y_{X/ATP}$ to the experimentally determined biomass yield coefficient $Y_{X/Glucose}$ using the detailed stoichiometric model.

D (h^{-1})	$Y_{X/Glucose}$ (g g^{-1})	$Y_{X/ATP}$ (g mol^{-1})	r_{ATP} (mmol g^{-1} h^{-1})
0·044	0·51	10·6	6·95
0·066	0·51	10·5	9·08
0·134	0·53	11·6	14·34
0·150	0·52	12·0	15·26
0·170	0·52	11·4	17·77
0·203	0·54	12·5	19·05
0·265	0·53	12·8	23·48
0·280	0·55	13·2	24·09
0·300	0·55	13·2	25·61
0·347	0·57	13·7	28·14
0·375	0·59	15·4	27·19
0·388	0·60	16·7	26·09
0·397	0·55	14·3	30·60

The determination of $Y_{X/ATP}$ at different dilution rates using the detailed stoichiometric model revealed increasing values of $Y_{X/ATP}$ with increasing dilution rates (Table 3), indicating more energy-efficient biomass formation at higher growth rates, i.e. less ATP consumption for biomass generation, presumably caused by less futile cycling, leaks and growth-associated maintenance. With known values of $Y_{X/ATP}$, the specific ATP production rate was calculated according to equation 9. Again, the deviation of the ATP production rate from the linear increase to lower values at dilution rates above 0·3 h^{-1} illustrates the more efficient ATP utilization at higher growth rates (Fig. 4). The energetic status of the cells was further investigated by determination of the AEC. The results revealed a decreasing AEC with increasing specific growth rate (Fig. 4). Above D = 0·3 h^{-1} there was a strong decline of the AEC, which remained nearly constant at 0·7 with further increasing dilution rates. The AEC plays a regulatory role in balancing

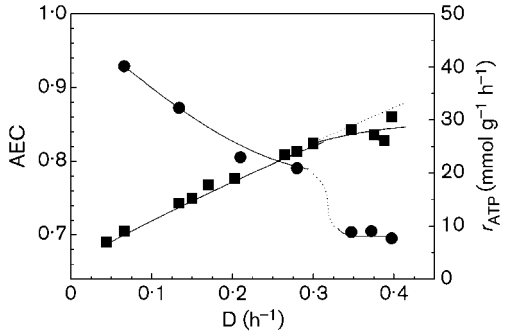

Fig. 4. Growth energetics during glucose-limited continuous culture of *E. coli* TG1. The ATP formation rate r_{ATP} (■) (Table 3) and the AEC (●) as functions of the dilution rate D. Data from dilution rates above 0·4 h^{-1} were omitted from these calculations.

the energy-forming and energy-utilizing reactions; a low energy charge most likely will repress ATP-consuming reactions, e.g. futile cycling, which allows metabolic activities to adapt more efficiently to the anabolic demands.

Altogether, the above results strongly suggest that the cell metabolism undergoes different types of carbon limitation with increasing dilution rates in a glucose-limited chemostat culture. Increasing growth rates first result in a more efficient use of the carbon substrate for biomass production, i.e. a larger portion of the carbon substrate is incorporated into biomass and a smaller portion is used in the respiratory, energy-generating pathway, concomitant with a low energetic status of the cells reflected by a low AEC.

Based on the detailed stoichiometric model, the metabolic flux distribution was determined at low (D = 0·066 h^{-1}) and high (D = 0·375 h^{-1}) dilution rates under conditions of cell-carbon and energy-carbon limitation, respectively (Fig. 5). With increasing dilution rate, the flux through the oxidative PP pathway increased at the expense of the flux through the EMP pathway and the TCA cycle. The excess carbon flux in the PP pathway is channelled back to the EMP pathway via the non-oxidative transaldolase- (r40) and transketolase- (r41) catalysed reactions. At the level of glyceraldehyde 3-phosphate (GAP; r7), 168 % mol mol^{-1} at D = 0·066 h^{-1} and 157 % mol mol^{-1} at D = 0·375 h^{-1} enter the EMP pathway. Thus, the carbon which is used for

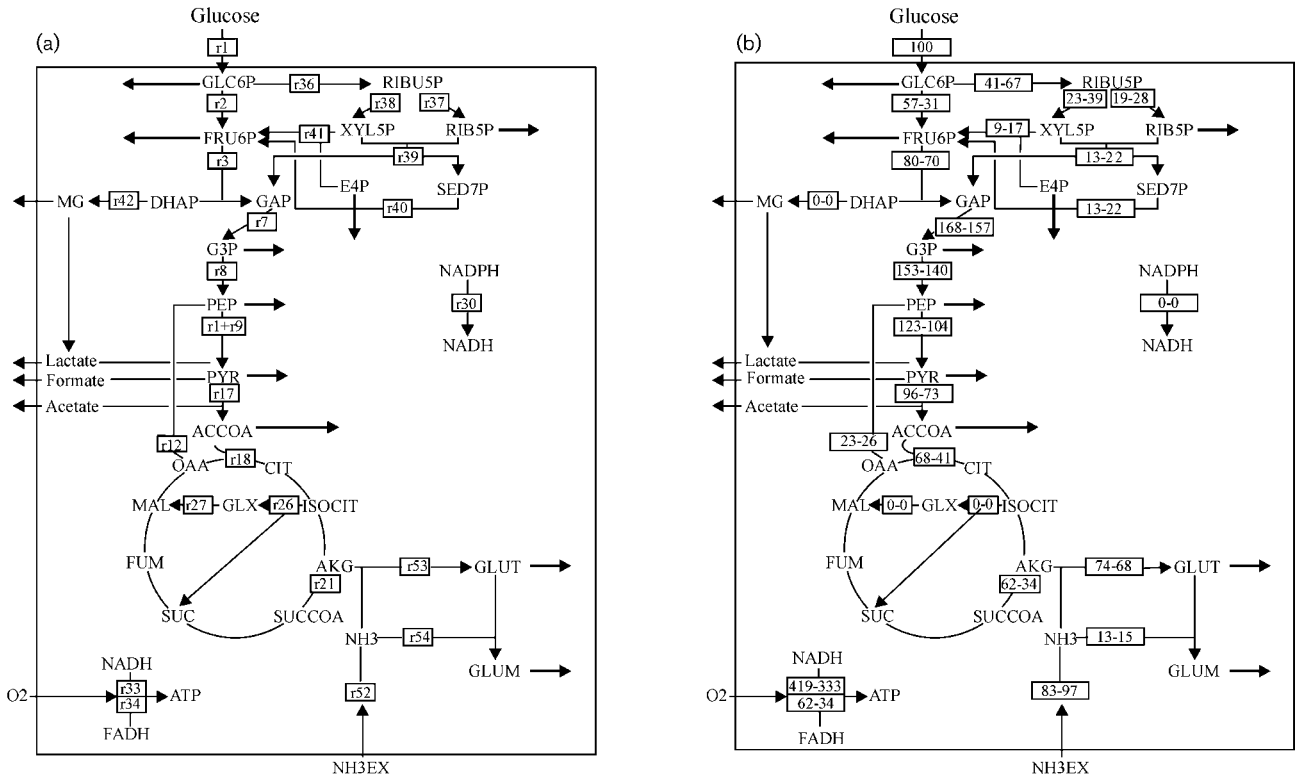

Fig. 5. Metabolic network of *E. coli* growing on glucose. (a) Reactions represented by numbers as given in the Appendix (detailed stoichiometric model). Not all reactions are displayed. (b) Metabolic flux distributions during growth under glucose-limited continuous-culture conditions at D = 0·066 h^{-1} (numbers on the left) and 0·375 h^{-1} (numbers on the right). All fluxes are expressed on a molar basis and are normalized with respect to the glucose uptake rate ($r_j\, r_{Glucose}{}^{-1} \times 100$ in % mol mol^{-1}; $r_{Glucose}$ = 0·73 mmol g^{-1} h^{-1} or 0·131 g g^{-1} h^{-1} for D = 0·066 h^{-1} and 3·56 mmol g^{-1} h^{-1} or 0·640 g g^{-1} h^{-1} for D = 0·375 h^{-1}).

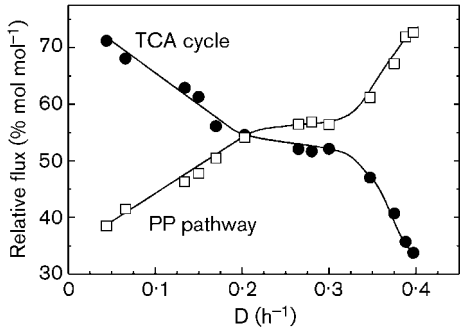

Fig. 6. Catabolic and anabolic flux distributions during glucose-limited continuous culture of *E. coli* TG1. Estimations of the metabolic flux through the TCA cycle (●) (r18) and the PP pathway (□) (r36) as functions of the dilution rate D. Fluxes are normalized with respect to the glucose uptake rate.

biomass and CO_2 formation up to the GAP level increases from 16 to 22 %. At the higher dilution rate, less carbon enters the TCA cycle. The resulting decreased NADH production rate decreases the ATP formation rate in the respiratory chain (r33 and r34) by 24 %. Alternative pathways such as the MG pathway (r42) or the glyoxylate shunt (r27 and r28) are not predicted to function in glucose-limited cultures under steady-state conditions. The MG pathway is most likely only activated under conditions of glucose excess (see accompanying paper; Weber *et al.*, 2005) and the glyoxylate shunt may not function in *E. coli* K-12 strains, as has been shown experimentally (^{13}C labelling) for the *E. coli* K-12 strain JM109 (Noronha *et al.*, 2000; Phue & Shiloach, 2004), a close relative of the *E. coli* K-12 strain TG1 (Sambrook *et al.*, 1989) employed in this study.

The fluxes through the TCA cycle (r18) and PP pathway (r36) are shown in Fig. 6 as functions of the dilution rate. The PP pathway flux (r36) increases from 39 % mol mol^{-1} to 73 % mol mol^{-1} with increasing dilution rate, showing the most prominent increase above a dilution rate of 0·3 h^{-1}. The TCA cycle flux (r18) behaves inversely and decreases from 71 % mol mol^{-1} to 34 % mol mol^{-1} with increasing dilution rate. In this context, it is important to note that the flux results obtained by the metabolite balancing approach also include the cofactor balance for NADH and NADPH. The NADPH balance forces the PP pathway to operate only to satisfy the biosynthetic demands for NADPH and pentose precursors. Flux measurements in *E. coli* using ^{13}C-labelled glucose which are not dependent on NADPH stoichiometries are in close agreement with the above analysis: a PP pathway flux of 53 % mol mol^{-1} and a TCA cycle flux of 45 % mol mol^{-1} have been reported (Schmidt *et al.*, 1999). Thus, the PP pathway utilization is intensified at the cost of the TCA cycle activity when growth rates increase in glucose-limited chemostat cultures. This change in the distribution of the metabolic pathway utilization is connected to an increased energy efficiency of carbon substrate utilization for biomass production. Also, one should recall that phosphoglucose-isomerase-negative mutants of *E. coli* (r2 not possible) are able to grow on glucose, although at slower rates compared with wild-type cells but with a higher biomass yield (Fraenkel & Vinopal, 1973; Canonaco *et al.*, 2001; Hua *et al.*, 2003), indicating that the function of the PP pathway extends beyond the supply of NADPH and biosynthetic precursors. Moreover, studies on *E. coli* gene-knockout mutants deficient in catabolic enzymes indicate a rather robust and flexible metabolic network, where pathways can substitute for each other, sometimes without significantly affecting growth rates (e.g. Zhao *et al.*, 2004). The feasibility of using the detailed stoichiometric model for prediction of reliable flux distributions was further validated by proving its ability to predict the measured respiratory rates; the relative deviation for r_{O_2} and r_{CO_2} was less than 10 % (Table 4).

Conclusions

Glucose is used as a cell-mass precursor and energy source. Thus, two types of limitations can occur: cell-carbon or energy-carbon limitation. Our data reveal a shift from cell-carbon limitation at low dilution rates to energy-carbon limitation at high dilution rates. This shift is accompanied

Table 4. Specific rates of carbon dioxide evolution and oxygen uptake determined from experimental data (Table 2) and predicted according to the detailed stoichiometric model and the relative deviation for glucose-limited continuous culture at dilution rates D = 0·066 h^{-1} and 0·375 h^{-1}

Rate (g g^{-1} h^{-1})	D = 0·066 h^{-1}				D = 0·375 h^{-1}		
	From experimental data	Model prediction	%	Wrong estimate*	From experimental data	Model prediction	%
r_{CO_2}	0·087	0·084	3·4	0·831	0·332	0·327	1·5
r_{O_2}	0·057	0·056	1·8	0·600	0·242	0·209	13·6

*The wrong estimate serves as a control for the response of the network. These values were calculated assuming a glucose uptake rate corresponding to D = 0·375 h^{-1}.

by an altered energetic state. At high dilution rates, a lowered specific ATP production rate and a drop of the AEC are observed. Moreover, this shift is accompanied by an increased flux through the PP pathway at the cost of the TCA cycle flux. Increasing limitations in the TCA cycle or in the respiratory chain with increasing growth rates concomitant with a more flexible PP pathway may cause the shift from cell-carbon to energy-carbon limitation at high dilution rates, resulting in a more energy-efficient conversion of glucose carbon into biomass.

At very high growth rates close to the wash-out point, the energy limitation becomes more severe, leading to the formation of acetate as an alternative route for energy generation through substrate-level phosphorylation. Energy generation through acetate formation yields less ATP compared with complete oxidation of the sugar carbon substrate; however, this route for energy generation appears to be the result of maximized energy generation under conditions of restrictions in the TCA cycle or in respiratory NADH turnover.

Although a detailed mechanism of acetate formation in aerobic cultures remains unknown, different hypotheses have been suggested for its formation by *E. coli* under 'carbon-overflow' conditions. All attribute acetate formation either to limitations in respiratory NADH turnover and concomitant ATP generation through oxidative phosphorylation (Andersen & von Meyenburg, 1980; Doelle *et al.*, 1982; Reiling *et al.*, 1985; Varma & Palsson, 1994) or to initial limitations in the TCA cycle (Majewski & Domach, 1990; Han *et al.*, 1992). Moreover, Han *et al.* (1992) concluded that these limitations cause a reorganization of the catabolic flux distribution to meet the anabolic demands at high growth rates by generating the necessary amount of energy by using both oxidative metabolism and acetic acid formation.

Such an reorganization of metabolism was observed in *E. coli* TG1 with increasing dilution rates. During the shift from cell-carbon to energy-carbon limiting conditions, the anabolic requirements are met first by a more efficient and less energy-consuming way of biomass formation by reduced TCA cycle activity and increased PP pathway flux, and, at even higher growth rates, by the activation of an alternative but less-efficient pathway for energy generation through substrate-level phosphorylation and concomitant formation of acetate.

APPENDIX

Simple stoichiometric model including catabolic and anabolic reactions

Reactions:

v_{cat}) $CH_2O \rightarrow 2\ H_2 + 0{\cdot}667\ ATP + CO_2$ (I)

v_{op}) $H_2 + 0{\cdot}5\ O_2 \rightarrow P/O\ ATP$ (II)

μ) $\beta_{Glucose/X} CH_2O + \beta_{N/X} NH_3 + \frac{1}{Y_{X/ATP}} ATP + \beta_{H/X} H_2 \rightarrow CH_{1{\cdot}85}O_{0{\cdot}574}N_{0{\cdot}22} + \beta_{CO_2/X}\ CO_2$ (III)

m_{ATP}) $ATP \rightarrow$ diss. (IV)

For catabolism, reactions of the EMP pathway and TCA cycle were lumped together. NADH and NADPH were considered as reducing equivalents 'H_2' and account for 10 moles per mole glucose oxidized. FADH was considered to account for 2 moles H_2 per mole glucose oxidized. Oxidative phosphorylation was described with the assumption that only NADH, not NADPH, can be oxidized. An energy dissipation reaction (m_{ATP}) was included to account for all ATP not consumed for biomass (X) formation.

Mass balances:

$$\begin{pmatrix} r_{ATP} \\ r_{H_2} \\ r_{Glucose} \\ r_{O_2} \\ r_{CO_2} \end{pmatrix} = \begin{pmatrix} -\frac{1}{Y_{X/ATP}} & 0{\cdot}667 & P/O & -1 \\ \beta_{H/X} & 2 & -1 & 0 \\ \beta_{Glucose/X} & 1 & 0 & 0 \\ 0 & 0 & 0{\cdot}5 & 0 \\ \beta_{CO_2/X} & 1 & 0 & 0 \end{pmatrix} \cdot \begin{pmatrix} \mu \\ v_{cat} \\ v_{op} \\ m_{ATP} \end{pmatrix} = \begin{pmatrix} 0 \\ 0 \\ r_{Glucose} \\ r_{O_2} \\ r_{CO_2} \end{pmatrix} \quad (10)$$

From the reaction rates, balances for the metabolites and cofactors can be generated. By eliminating the reaction rates v_{cat} and v_{op}, an equation for the glucose uptake rate $r_{Glucose}$ was obtained which can be coupled to the model of Pirt (1965):

$$r_{Glucose} = \left(\frac{\frac{1}{Y_{X/ATP}} - P/O{\cdot}\beta_{H/X}}{0{\cdot}667 + 2{\cdot}P/O} + \beta_{Glucose/X} \right) \cdot \mu + \frac{m_{ATP}}{0{\cdot}667 + 2{\cdot}P/O} = \frac{\mu}{Y^{true}_{X/Glucose}} + m_{Glucose} \quad (11)$$

From equation 11, equations for $Y_{X/ATP}$ and m_{ATP} can be derived:

$$\frac{1}{Y_{X/ATP}} = \left(\frac{2}{Y^{true}_{X/Glucose}} - 2{\cdot}\beta_{Glucose/X} + \beta_{H/X} \right) \cdot P/O + \frac{0{\cdot}667}{Y^{true}_{X/Glucose}} - 0{\cdot}667{\cdot}\beta_{Glucose/X} \quad (12)$$

$$m_{ATP} = m_{Glucose} \cdot (0{\cdot}667 + 2{\cdot}P/O) \quad (13)$$

Parameters:

$Y^{true}_{X/Glucose} = 0{\cdot}581$ C-mol C-mol^{-1} ($0{\cdot}574$ g g^{-1}), $m_{Glucose} = 0{\cdot}02$ C-mol C-mol^{-1} h^{-1} ($0{\cdot}02$ g g^{-1} h^{-1}); parameter determined from experimental data for the linear range $D = 0 \rightarrow 0{\cdot}347$ h^{-1} (Table 2).

$\beta_{Glucose/X} = 1{\cdot}174$ C-mol C-mol^{-1}, $\beta_{H/X} = 0{\cdot}159$ mol C-mol^{-1}; ratio determined by a stoichiometric analysis of the (macromolecular) biomass composition as described in Nielsen & Villadsen (1994) (p. 106 ff.).

$P/O = 1{\cdot}75$ (according to Zeng *et al.*, 1990).

Detailed stoichiometric model

Reactions in the biochemical network:

Reactions are indicated as reversible (=) or irreversible ($\Rightarrow$).

Phosphotransferase system

r1) $GLC + PEP \Rightarrow GLC6P + PYR$

EMP pathway

r2) $GLC6P = FRU6P$

r3) $FRU6P + ATP \Rightarrow FRU16P$

r4) FRU16P⇒FRU6P

r5) FRU16P = GAP + DHAP

r6) DHAP = GAP

r7) GAP = NADH + G3P + ATP

r8) G3P = PEP

r9) PEP⇒ATP + PYR

r10) PYR + ATP⇒PEP

PEP carboxykinase and PEP carboxylase

r11) OAA + ATP⇒PEP + CO2

r12) PEP + CO2⇒OAA

By-products

r13) PYR = ACCOA + FORM

r14) ACCOA = AC + ATP

r15) 2 ATP + AC⇒ACCOA

r16) ACCOA + 2 NADH⇒ETOH

r17) PYR⇒ACCOA + CO2 + NADH

TCA cycle

r18) ACCOA + OAA⇒CIT

r19) CIT = ISOCIT

r20) ISOCIT = AKG + NADPH + CO2

r21) AKG⇒SUCCOA + CO2 + NADH

r22) SUCCOA = ATP + SUC

r23) SUC⇒FADH + FUM

r24) FUM = MAL

r25) MAL⇒OAA + NADH

Glyoxylate shunt

r26) ISOCIT⇒SUC + GLX

r27) ACCOA + GLX⇒MAL

r28) MAL⇒PYR + CO2 + NADPH

r29) MAL⇒PYR + CO2 + NADH

Transhydrogenation

r30) NADPH⇒NADH

r31) NADH + PO ATP⇒NADPH

Oxidative phosphorylation

r32) NADH + 0·5 O2⇒PO ATP

r33) NADH + 0·5 O2⇒2 PO ATP

r34) FADH + 0·5 O2⇒PO ATP

r35) FORM + 0·5 O2⇒PO ATP + CO2

PP pathway

r36) GLC6P⇒RIBU5P + CO2 + 2 NADPH

r37) RIBU5P = RIB5P

r38) RIBU5P = XYL5P

r39) XYL5P + RIB5P = SED7P + GAP

r40) SED7P + GAP = FRU6P + E4P

r41) XYL5P + E4P = FRU6P + GAP

MG pathway

r42) DHAP⇒MG

r43) MG + NADPH = LACALD

r44) MG + GLUTH = LACTGL

r45) LACTGL = DLAC + GLUTH

r46) MG⇒DLAC

r47) PYR + NADH⇒DLAC

r48) DLAC⇒PYR + FADH

r49) LACALD⇒LLAC + NADH

r50) PYR + NADH⇒LLAC

r51) LLAC⇒PYR + FADH

Ammonium, glutamate and glutamine

r52) NH3EX + 0·5 ATP = NH3

r53) NH3 + AKG + NADPH = GLUT

r54) GLUT + NH3 + ATP = GLUM

Amino acids

r55) NADPH + ATP + 2 GLUT + ACCOA⇒AKG + AC + ORN

r56) CO2 + GLUM + 2 ATP = GLUT + CAP

r57) CAP + ORN = CR

r58) ATP + ASP + CR = FUM + ARG

r59) GLUT + G3P = NADH + AKG + SER

r60) SER + ACCOA + H2S = CYS + AC

r61) SER = NNMTHF + GLY

r62) OAA + GLUT = ASP + AKG

r63) 2 ATP + GLUM + ASP = ASN + GLUT

r64) 2 NADPH + ATP + ASP = HSER

r65) SUCCOA + CYS + HSER = SUC + PYR + NH3 + HCYS

r66) NMTHF + HCYS = MET

r67) ATP + HSER = THR

r68) NADPH + 2 PYR = CO2 + AKI

r69) AKI + GLUT = AKG + VAL

r70) AKI + ACCOA + GLUT = LEU + AKG + NADH + CO2

r71) GLUT + PYR = AKG + ALA

r72) NADPH + PYR + GLUT + THR = CO2 + NH3 + AKG + ILE

r73) ATP + NADPH + E4P + 2 PEP⇒CHOR

r74) CHOR + GLUM + SER + PRPP⇒
TRP + GLUT + PYR + GAP + CO2

r75) CHOR = PREPH

r76) PREPH + GLUT⇒CO2 + AKG + TYR + NADH

r77) GLUT + PREPH⇒CO2 + AKG + PHE

r78) GLUM + ATP′ + PRPP⇒2 NADH + AICAR + AKG + HIS

r79) GLUT + ATP + 2 NADPH⇒PRO

r80) ASP + PYR + 2 NADPH + SUCCOA + GLUT + ATP⇒SUC + AKG + CO2 + LYS

Protein

r81) 1·18 ATP + 0·042 VAL + 0·005 TRP + 0·013 TYR + 0·024 THR + 0·021 SER + 0·021 PRO + 0·018 PHE + 0·015 MET + 0·033 LYS + 0·043 LEU + 0·028 ILE + 0·009 HIS + 0·059 GLY + 0·025 GLUM + 0·025 GLUT + 0·009 CYS + 0·023 ASP + 0·023 ASN + 0·028 ARG + 0·049 ALA = PROTEIN

Nucleotides

r82) NFTHF + AICAR = IMP

r83) IMP + ASP + 3 ATP = ATP′ + MAL

r84) IMP + GLUM + 4 ATP = GTP + GLUT + NADH

r85) 4 ATP + GLUM + ASP + PRPP = UTP + GLUT + NADH

r86) ATP + GLUM + UTP = GLUT + CTP

RNA

r87) 0·0165 ATP′ + 0·0203 GTP + 0·0136 UTP + 0·0126 CTP + 0·0256 ATP = RNA

DNA

r88) 0·00247 ATP′ + 0·00247 UTP + 0·00254 GTP + 0·00254 CTP + 0·015 ATP = DNA

Lipids

r89) 0·0129 PAL + 0·0129 OL + 0·0129 GAP + 0·0129 SER + 0·0258 ATP = LIPID

r90) 8 ACCOA + 7 ATP + 13 NADPH = PAL

r91) 9 ACCOA + 9 ATP + 15 NADPH = OL

Lipopolysaccharide

r92) 0·00509 GLC6P + 0·0481 ATP + 0·0376 NADPH + 0·033 ACCOA + 0·0023 RIB5P + 0·0023 PEP + 0·00392 GLUT + 0·00235 G3P = LPS + 0·0023 NADH + 0·00392 AKG

Peptidoglycan

r93) 0·00276 FRU6P + 0·0055 ACCOA + 0·00276 PEP + 0·00276 PYR + 0·00276 OAA + 0·02484 ATP + 0·0193 GLUT + 0·0193 NADPH = PG + 0·0138 AKG

Glycogen

r94) 0·0154 GLC6P + 0·0154 ATP = GLYC

One-carbon units and polyamine

r95) 0·00485 SER = C1

r96) 0·0119 ATP + 0·01779 NADPH + 0·0119 GLUT = PA + 0·01397 AKG

Biomass

r97) 1·12 PROTEIN + 0·56 RNA + LIPID + LPS + GLYC + PG + DNA + C1 + PA + $\frac{1}{Y_{X/ATP}}$ ATP = BIOMASS

Miscellaneous

r98) NNMTHF + NADH = NMTHF

r99) GLY = NADH + CO2 + NH3 + NNMTHF

r100) 2 ATP + RIB5P = PRPP

r101) PRPP + GLY + ASP + NFTHF + CO2 + 4 ATP = AICAR + MAL + 2 GLUT

r102) NNMTHF = NADPH + NFTHF

Objective

r103) BIOMASS

Metabolite accumulation rate vector:

1) AC Acetate

2) ACCOA Acetyl coenzyme A

3) AICAR Aminoimidazole carboxamide ribonucleotide

4) AKG α-Ketoglutarate

5) AKI α-Ketoisovalerate

6) ALA Alanine

7) ARG Arginine

8) ASN Asparagine

9) ASP Aspartate

10) ATP Adenosine 5′-triphosphate (energy source)

11) ATP′ Adenosine 5′-triphosphate (nucleotide for RNA and DNA)

12) BIOMASS Biomass

13) C1 One-carbon unit

14) CAP Carbamoyl phosphate

15) CHOR Chorismate

16) CIT Citrate

17) CO2 Carbon dioxide

18) CR Citrulline

19) CTP Cytidine 5′-triphosphate

20) CYS Cysteine

21) DHAP Dihydroxyacetone phosphate

22) DLAC D-Lactate

23) DNA Deoxyribonucleic acid

24) E4P Erythrose 4-phosphate

25) ETOH Ethanol

26) FADH Flavin adenine dinucleotide, reduced

27) FORM Formate

28) FRU16P Fructose 1,6-bisphosphate

29) FRU6P Fructose 6-phosphate

30) FUM Fumarate

31) G3P 3-Phosphoglycerate

32) GAP Glyceraldehyde 3-phosphate

33) GLC Glucose

34) GLC6P Glucose 6-phosphate

35) GLUM Glutamine

36) GLUT Glutamate

37) GLX Glyoxylate

38) GLY Glycine

39) GLYC Glycogen

40) GTP Guanidine 5′-triphosphate

41) HCYS Homocysteine

42) HIS Histidine

43) HSER Homoserine

44) ILE Isoleucine

45) IMP Inosine 5′-monophosphate

46) ISOCIT Isocitrate

47) LACALD Lactaldehyde

48) LACTGL Lactoylglutathione

49) LEU Leucine

50) LIPID Lipid

51) LLAC L-Lactate

52) LPS Lipopolysaccharide

53) LYS Lysine

54) MAL Malate

55) MET Methionine

56) MG Methylglyoxal

57) NADH Nicotinamide adenine dinucleotide, reduced

58) NADPH Nicotinamide adenine dinucleotide phosphate, reduced

59) NFTHF N^{10}-formyl tetrahydrofolate

60) NH3 Ammonia

61) NH3EX Ammonia, extracellular

62) NMTHF N^{5}-methenylformyl tetrahydrofolate

63) NNMTHF N^{5}-N^{10}-methyleneformyl tetrahydrofolate

64) O2 Oxygen

65) OAA Oxaloacetate

66) OL Oleate

67) ORN Ornithine

68) PA Polyamine

69) PAL Palmitoleate

70) PEP Phosphoenolpyruvate

71) PG Peptidoglycan

72) PHE Phenylalanine

73) PREPH Prephenate

74) PRO Proline

75) PROTEIN Protein

76) PRPP 5-Phosphoribosyl 1-pyrophosphate

77) PYR Pyruvate

78) RIB5P Ribose 5-phosphate

79) RIBU5P Ribulose 5-phosphate

80) RNA Ribonucleic acid

81) SED7P Sedoheptulose 7-phosphate

82) SER Serine

83) SUC Succinate

84) SUCCOA Succinyl CoA

85) THR Threonine

86) TRP Tryptophan

87) TYR Tyrosine

88) UTP Uridine 5′-triphosphate

89) VAL Valine

90) XYL5P Xylulose 5-phosphate

For simplicity, the oxidized forms of the cofactors NADP, NAD and FAD and also ADP are not shown in the reactions of the biochemical network. Moreover, these compounds are not included in the metabolite balance because of lack of information gain. Also, glutathione (GLUTH, r44 and r45) and H_2S (r60) are shown in the biochemical network but were not included in the metabolite balance. Moreover, uridine 5′-triphosphate (UTP) is considered to be equivalent to thymidine 5′-triphosphate (TTP) in the biochemical network.

ACKNOWLEDGEMENTS

We gratefully acknowledge financial support by the Volkswagenstiftung (I/69 816). Also, we are grateful to Klaus Gollmer for providing the MATLAB modelling and Simulation Toolbox and to Bernd Hitzmann for fruitful discussions. We also like to thank Rutger de Wit and the anonymous reviewers for their helpful suggestions concerning this manuscript.

REFERENCES

Andersen, K. B. & von Meyenburg, K. (1980). Are growth rates of *Escherichia coli* in batch cultures limited by respiration? *J Bacteriol* **144**, 114–123.

Atkinson, D. E. (1968). The energy charge of the adenylate pool as a regulatory parameter. Interaction with feedback modifiers. *Biochemistry* **7**, 4030–4034.

Bauchop, T. & Elsden, S. R. (1960). The growth of micro-organisms in relation to their energy supply. *J Gen Microbiol* **23**, 457–469.

Benthin, S., Nielsen, J. & Villadsen, J. (1991). A simple and reliable method for the determination of cellular RNA content. *Biotechnol Tech* **5**, 39–42.

Boonstra, B., French, C. E., Wainwright, I. & Bruce, N. C. (1999). The *udhA* gene of *Escherichia coli* encodes a soluble pyridine nucleotide transhydrogenase. *J Bacteriol* **181**, 1030–1034.

Bragg, P. D., Davies, P. L. & Hou, C. (1972). Function of energy-dependent transhydrogenase in *Escherichia coli*. *Biochem Biophys Res Commun* **47**, 1248–1255.

Canonaco, F., Hess, T. A., Heri, S., Wang, T., Szyperski, T. & Sauer, U. (2001). Metabolic flux response to phosphoglucose isomerase knock-out in *Escherichia coli* and impact of overexpression of the soluble transhydrogenase UdhA. *FEMS Microbiol Lett* **204**, 247–252.

Daae, E. B. & Ison, A. P. (1999). Classification and sensitivity analysis of a proposed primary metabolic reaction network for *Streptomyces lividans*. *Metab Eng* **1**, 153–165.

Doelle, H. W., Ewing, K. N. & Hollywood, N. W. (1982). Regulation of glucose metabolism in bacterial systems. *Adv Biochem Eng* **23**, 1–35.

Farmer, I. S. & Jones, C. W. (1976). The energetics of *Escherichia coli* during aerobic growth in continuous culture. *Eur J Biochem* **67**, 115–122.

Fraenkel, D. G. & Vinopal, R. T. (1973). Carbohydrate metabolism in bacteria. *Annu Rev Microbiol* **27**, 69–100.

Han, K., Lim, H. C. & Hong, J. (1992). Acetic acid formation in *Escherichia coli* fermentation. *Biotechnol Bioeng* **39**, 663–671.

Herbert, D., Phipps, P. J. & Strange, R. E. (1971). Chemical analysis of microbial cells. *Methods Microbiol* **5B**, 209–344.

Hoffmann, F. & Rinas, U. (2001). On-line estimation of the metabolic burden resulting from synthesis of plasmid-encoded and heat-shock proteins by monitoring respiratory energy generation. *Biotechnol Bioeng* **76**, 333–340.

Hua, Q., Yang, C., Baba, T., Mori, H. & Shimizu, K. (2003). Responses of the central metabolism in *Escherichia coli* to phosphoglucose isomerase and glucose-6-phosphate dehydrogenase knockouts. *J Bacteriol* **185**, 7053–7067.

Ingraham, J. L., Maaloe, O. & Neidhardt, F. C. (1983). Chemical synthesis of the bacterial cell: polymerization, biosynthesis, fueling reactions, and transport. In *Growth of the Bacterial Cell*, pp. 87–173. Sunderland, MA: Sinauer Associates.

Karp, P. D., Riley, M., Paley, S. M., Pellegrini-Toole, A. & Krummenacker, M. (1999). EcoCyc: encyclopedia of *Escherichia coli* genes and metabolism. *Nucleic Acids Res* **27**, 55–58.

Korz, D. J., Rinas, U., Hellmuth, K., Sanders, E. A. & Deckwer, W.-D. (1995). Simple fed-batch technique for high cell density cultivation of *Escherichia coli*. *J Biotechnol* **39**, 59–65.

Majewski, R. A. & Domach, M. M. (1990). Simple constrained-optimization view of acetate overflow in *E. coli*. *Biotechnol Bioeng* **35**, 732–738.

Nielsen, J. & Villadsen, J. (1994). *Bioreaction Engineering Principles*. New York: Plenum.

Noronha, S. B., Yeh, H. J. C., Spande, T. F. & Shiloach, J. (2000). Investigation of the TCA cycle and the glyoxylate shunt in *Escherichia coli* BL21 and JM109 using ^{13}C-NMR/MS. *Biotechnol Bioeng* **68**, 316–327.

Phue, J.-N. & Shiloach, J. (2004). Transcription levels of key metabolic genes are the cause for different glucose utilization pathways in *E. coli* B (BL21) and *E. coli* K (JM109). *J Biotechnol* **109**, 21–30.

Pirt, J. (1965). The maintenance energy of bacteria in growing cultures. *Proc R Soc Lond B Biol Sci* **163**, 224–231.

Pramanik, J. & Keasling, J. D. (1997). Stoichiometric model of *Escherichia coli* metabolism: incorporation of growth-rate dependent biomass composition and mechanistic energy requirements. *Biotechnol Bioeng* **56**, 398–421.

Reiling, H. E., Laurila, H. & Fiechter, A. (1985). Mass culture of *Escherichia coli*: medium development for low and high density cultivation of *Escherichia coli* B/r in minimal and complex media. *J Biotechnol* **2**, 191–206.

Riesenberg, D., Schulz, V., Knorre, W. A., Pohl, H.-D., Korz, D., Sanders, E. A., Roß, A. & Deckwer, W.-D. (1991). High cell density cultivation of *Escherichia coli* at controlled specific growth rate. *J Biotechnol* **20**, 17–27.

Rydström, J. (1977). Energy-linked nicotinamide nucleotide transhydrogenases. *Biochim Biophys Acta* **463**, 155–184.

Ryll, T. & Wagner, R. (1991). Improved ion-pair high-performance liquid chromatographic method for the quantification of a wide variety of nucleotides and sugar-nucleotides in animal cells. *J Chromatogr* **570**, 77–88.

Sambrook, J., Fritsch, E. F. & Maniatis, T. (1989). *Molecular Cloning: a Laboratory Manual*, 2nd edn. Cold Spring Harbor, NY: Cold Spring Harbor Laboratory.

Schmidt, K., Nielsen, J. & Villadsen, J. (1999). Quantitative analysis of metabolic fluxes in *Escherichia coli*, using two-dimensional NMR spectroscopy and complete isotopomer models. *J Biotechnol* **71**, 175–189.

Shahab, N., Flett, F., Oliver, S. G. & Butler, P. R. (1996). Growth rate control of protein and nucleic acid content in *Streptomyces coelicolor* A3(2) and *Escherichia coli* B/r. *Microbiology* **142**, 1927–1935.

Stouthamer, A. H. (1973). A theoretical study on the amount of ATP required for synthesis of microbial cell material. *Antonie van Leeuwenhoek* **39**, 545–565.

Stouthamer, A. H. & Bettenhaussen, C. (1973). Utilization of energy for growth and maintenance in continuous and batch cultures of microorganisms. A reevaluation of the method for the determination of ATP production by measuring molar growth yields. *Biochim Biophys Acta* **301**, 53–70.

Theobald, U., Mailinger, W., Baltes, M., Rizzi, M. & Reuss, M. (1997). *In vivo* analysis of metabolic dynamics in *Saccharomyces cerevisiae*. I. Experimental observations. *Biotechnol Bioeng* **55**, 305–316.

Vallino, J. J. & Stephanopoulos, G. (1990). Flux determination in cellular bioreaction networks: applications to lysine fermentations. In *Frontiers in Bioprocessing*, pp. 205–219. Edited by S. K. Sikdar, M. Bier & P. Todd. Boca Raton, FL: CRC Press.

van Gulik, W. M. & Heijnen, J. J. (1995). A metabolic network stoichiometry analysis of microbial growth and product formation. *Biotechnol Bioeng* **48**, 681–698.

Varma, A. & Palsson, B. O. (1993). Metabolic capabilities of *Escherichia coli*. II. Optimal growth patterns. *J Theor Biol* **165**, 503–522.

Varma, A. & Palsson, B. O. (1994). Stoichiometric flux balance models quantitatively predict growth and metabolic by-product secretion in wild-type *Escherichia coli* W3110. *Appl Environ Microbiol* **60**, 3724–3731.

Weber, J., Hoffmann, F. & Rinas, U. (2002). Metabolic adaptation of *Escherichia coli* during temperature-induced recombinant protein synthesis: 2. Redirection of metabolic fluxes. *Biotechnol Bioeng* **80**, 320–330.

Weber, J., Kayser, A. & Rinas, U. (2005). Metabolic flux analysis of *Escherichia coli* in glucose-limited continuous culture. II. Dynamic response to famine and feast, activation of the methylglyoxal pathway and oscillatory behaviour. *Microbiology* **151**, 707–716.

Zeng, A. P., Ross, A. & Deckwer, W.-D. (1990). A method to estimate the efficiency of oxidative phosphorylation and biomass yield from ATP of a facultative anaerobe in continuous culture. *Biotechnol Bioeng* **36**, 965–969.

Zhao, J., Baba, T., Mori, H. & Shimizu, K. (2004). Global metabolic response of *Escherichia coli* to *gnd* or *zwf* gene-knockout, based on ^{13}C-labeling experiments and the measurement of enzyme activities. *Appl Microbiol Biotechnol* **64**, 91–98.